Openmouthed β-SiC hollow-sphere with highly photocatalytic activity for reduction of CO$_2$ with H$_2$O

Ying Wang [a], Lina Zhang [a], Xiaoyan Zhang [a], Zizhong Zhang [a,*], Yuecong Tong [a], Fuying Li [a], Jeffrey C.-S. Wu [b], Xuxu Wang [a,*]

[a] State Key Laboratory of Photocatalysis on Energy and Environment, Research Institute of Photocatalysis, College of Chemistry, Fuzhou University, PR China
[b] Department of Chemical Engineering, National Taiwan University, Taipei 10617, Taiwan

ARTICLE INFO

ABSTRACT

A novel hollow spherical 3D structure of β-SiC with an open mouth was successfully fabricated by an environmentally friendly approach starting from ethylsilicate interaction with the P123 and glucose. The proposed growth mechanism of SiC hollow spheres was revealed step by step with SEM and XRD. When the as-prepared SiC was applied for the photocatalytic reduction of CO$_2$ with pure water, it was found to be highly active for the conversion CO$_2$ into mainly CH$_4$ hydrocarbon products due to its unique electronic structure, hollow morphology and high BET surface area. Moreover, the photocatalytic activity of the hollow spherical SiC can be greatly improved by loading Pt cocatalyst. The optimal 2.0 wt% Pt loading led to a stable CH$_4$ evolution as high as 16.8 μmol/g/h (or 376.4 μl/g/h) with the simulated solar light irradiation, which is higher than that of many reported metal oxides (Pt/TiO$_2$, CdS/WO$_3$, Zn$_2$GeO$_4$, CeO$_2$ and g-C$_3$N$_4$/NaNbO$_3$ et al.) under similar experimental conditions. This work provides a new strategy for the architecture of thermally and chemically stable non-metallic carbide with unique hollow spherical structure to be a potential nonmetallic photocatalyst for CO$_2$ reduction into CH$_4$.

© 2017 Elsevier B.V. All rights reserved.

1. Introduction

Harvesting solar energy for the photocatalytic conversion of CO$_2$ into chemical fuels is an ideal solution to address global warming and carbon cycle in nature. To achieve this objective reaction, many efforts have been devoted to developing efficient photocatalysts ranging from semiconducting materials, such as TiO$_2$, Zn$_2$GaO$_4$, CdS, and C$_3$N$_4$ [1], to metal–organic frameworks (MOFs) including NH$_2$-MIL-125(Ti) [2], Fe_MOF-525 [3], and Mn(bpydc)-(CO)$_3$Br [4]. However, the efficiency of photocatalytic CO$_2$ conversion is still very low even in the presence of electron donor sacrificial agent [5]. Searching for suitable photocatalyst materials for efficient CO$_2$ conversion is one of the fundamental missions in photocatalysis communications.

Silicon carbide (SiC), one of the very important non-metallic oxide semiconductors, has been applied widely from metallurgy to aerospace due to its high thermal conductivity and high strength [6–9]. On the other hand, SiC also possesses several other unique properties, including moderate wide of band gap of Eg ≈ 2.4 eV,

considerable negative conduction band potential (−1.40 V), high chemical stability and environmental friendliness. These make SiC suitable as a photocatalyst, especially for the high reduction potential reactions such as water reduction and CO$_2$ reduction in efficiently harvesting solar energy. Actually, SiC was reported to has good activity for photocatalytic splitting pure water under ultraviolet light irradiation as early as 1990 [10,11]. However, to the best of our knowledge, SiC has been only a few study as a photocatalyst in the CO$_2$ reduction up to date [12], although it is more suitable in electron structure than the majority of semiconductor materials.

The morphology commonly has a significant effect on the material properties and applications. One-, two-, and three-dimensional structure of SiC, such as nanofibers [13–17], whisker [18–20], monomolecular layers [21], and hollow spheres [22–26], have been fabricated by various approaches such as carbothermic method [27–29], chemical vapor deposition [30,31], template-directed process [32–34]. The morphologically controlling synthesis of SiC by a simple and friendly approach is still desirable. For diverse structures, the hollow spherical microstructure has attracted intensive attentions as a photocatalyst. Its high surface area, high porosity, low bulk density, and multi-reflections of light within interior cavities are considered to be very favorable for mass transfer and efficient utilization of solar light in the photocatalytic process.

* Corresponding authors.
E-mail addresses: z.zhang@fzu.edu.cn (Z. Zhang), xwang@fzu.edu.cn (X. Wang).

There has been many methods to be developed for the preparation of hollow spherical metal oxides and sulfides photocatalyst [35]. However, the synthesis of some hollow structure carbide and nitride materials remains a challenge due to high temperature calcination. Zhang et al. [24] prepared SiC hollow spheres by the solid–gas reaction of carbon spheres with excess micro-grade silicon at 1300 °C. Shen et al. [25] have succeeded in synthesizing SiC hollow microspheres by using $SiCl_4$ and C_6Cl_6 as source materials and metallic sodium as reductant. Zhou et al. [26] reported that the ordered SnO_2/SiC hollow sphere nanochains can be prepared through the topological morphology conversion of $C@SnO_2$ core–shell nanochains in a vapor–solid reaction process. However, these synthesis methods for hollow spherical SiC were involved toxic raw materials or a complicated procedure.

Herein, we report an openmouthed β-SiC hollow-Sphere. It was synthesized by environmentally friendly approach using frequently-used glucose as the carbon resource. The effect of the reaction temperature and time on the hollow sphere morphology was systemically investigated. The possible formation mechanism was suggested according to the analysis results of SEM and XRD. The as-prepared SiC hollow spheres was observed to show a much higher photocatalytic activity for the reduction of CO_2 with H_2O to CH_4 than the commercial SiC or the standard photocatalyst P25 TiO_2. These findings not only show that SiC material is a promising photocatalyst for CO_2 reduction, but also imply that photocatalytic behavior of SiC could be effectively modulated by morphology.

2. Experimental section

2.1. Materials

P123 (PEO-PPO-PEO) and $H_2PtCl_6·6H_2O$ were acquired from ALDRICH and Aladdin, respectively. Other reagents used in the present study, including ethanol, hydrochloric acid, TEOS (ethylsilicate), glucose, sodium hydroxide and methanol, were of analytical reagent grade and obtained from Sinopharm Chemical Reagent Co., Ltd. All of the above chemicals were used without further purification.

2.2. Preparation of SiC hollow sphere

SiC precursor was prepared by Sol-Gel method. In a typical preparation procedure, 2.53 g of P123 was added to the mixed solution containing 3 ml of deionized water, 2.4 ml of ethanol, and 0.3 ml of 1 M hydrochloric acid under magnetic stirring at room temperature until formation of a homogeneous solution. 6.4 ml of ethylsilicate and 10.8 g of glucose were then introduced to the above homogeneous solution by heating at 363 K for 12 h to get a yellow gel. The resulted yellow gel was dried in an oven at 393 K to obtain a brown aerogel SiC precursor.

The SiC samples were prepared by carbothermic reduction of the SiC precursor according to the following steps. Firstly, the brown aerogel SiC precursor was pre-carbonized in flowing N_2 atmosphere at 823 K for 5 h, and then shifted to flowing Ar atmosphere at high temperature (1723 or 1773 K) for a certain time (5, 8, or 10 h). Finally, the carbonized samples were calcined in O_2 atmosphere at 873 K for 5 h to remove residual carbon following by immersing in 10 wt% sodium hydroxide solution to remove unreacted SiO_2. The obtained SiC sample was washed with deionized water serval times and dried at 333 K. The obtained SiC samples were denoted as SiC (xK, yh), where x stands for carbothermic reduction temperature (x = 1723, 1773) and y represents carbothermic reduction time (y = 5, 8, 10).

2.3. Preparation of Pt/SiC

Pt loaded SiC samples (Pt/SiC) were prepared by using incipient-wetness impregnation method. In detail, 0.3 g of the as-prepared SiC (1723 K, 8 h) was added to an aqueous solution with different concentration of chloroplatinic acid. The suspended solution was under ultrasound for 0.5 h to ensure the absorption of chloroplatinic acid on SiC. And then the SiC solids were recovered by centrifugation and dried at 393 K for 5 h. The resulted samples were reduced with 0.1 M of sodium borohydride, followed by the deionized water washing and drying at 333 K. The obtained samples were denoted as z wt%Pt/SiC, where z stands for the weight percentage of the Pt species (z = 0, 1, 2, 3).

2.4. Characterization

The XRD patterns were recorded with Ni filtered Cu Kα radiation at 40 kV and 40 mA on a Bruker D8 Advance X-ray diffractometer. The morphology of sample was characterized by a field emission scanning electron microscopy (FESEM) (JSM-6700F), while the transmission electron microscopy (TEM) images were obtained at an accelerating voltage of 200 kV using a JEOL model JEM 2010 EX instrument. The thermo analysis (TG-DSC) was carried out by a NETSCHZ STA-449C thermoanalyzer with a heating rate of 10 K/min under argon atmosphere. The UV–vis diffuse reflectance (UV–vis DRS) spectra were obtained on a UV–vis spectrophotometer (Cary 500) with a self-supporting sample cell, and the pure $BaSO_4$ was used as a reflectance standard. Brunauer–Emmett–Teller (BET) surface area and CO_2 adsorption were measured with an ASAP2020M apparatus (Micromeritics Instrument Corp., USA). Nitrogen adsorption and desorption isotherms were measured at 77 K, and CO_2 adsorption isotherms were measured at 273 K. The elemental composition of samples was analyzed by X-ray photoelectron spectroscopy (XPS, VG, Physical Electrons Quantum 2000 Scanning Esca Microprob, Al Kα$_1$ radiation). The products of the $^{13}CO_2$ and $^{12}CO_2$ isotopic experiment were analyzed by Hiden HPR-20 mass spectrometer. Photoluminescence excitation spectra was recorded on a FL/FS920 spectrofluorimeter (Edinburgh Instruments) fluorescence spectrometer at room temperature, the excitation wavelength is 375 nm.

2.5. Photocatalytic activity measurement

Photocatalytic reduction of CO_2 in the presence of H_2O was carried out as a gas–solid heterogeneous reaction in a 40 ml Schlenk tube with a silicone rubber septum under atmospheric pressure at ambient temperature (298 K). The light source was a 300 W commercial Xe lamp vertically placed outside the reactor. 10 mg of photocatalyst was placed into the reaction tube. The system was evacuated by a mechanical pump and then filled with pure CO_2 gas. This evacuation–filling operation was repeated three times. Finally, 1 ml of pure water was added into the reactor via the silicone rubber septum. The photocatalytic reaction was typically performed for 4 h. After light irradiation, the amount of CH_4 formed was analyzed using a GC-7890A gas chromatograph equipped with a FID detector and a capillary column (GC-GASPRO, 30 m × 0.320 mm). The generated O_2 was detected by HP 7890 gas chromatography (Ar carrier) equipped with a TCD detector and 5A molecular sieve packed column (10 m × 2 mm).

2.6. Photoelectrochemical measurements

Photoelectrochemical measurements were carried out with a BAS Epsilon workstation using a standard three-electrode electrochemical cell with a working electrode, a platinum foil as the counter electrode, and a saturated Ag/AgCl electrode as the refer-
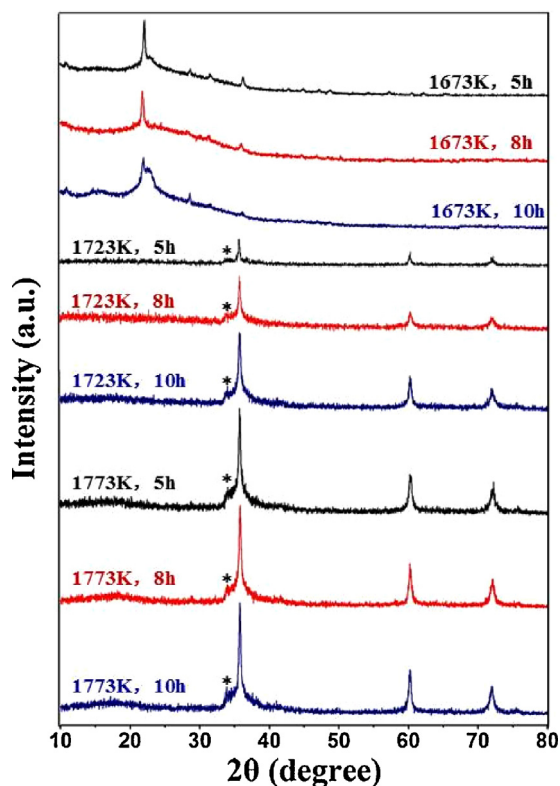
Fig. 1. XRD patterns of samples carbothermic reduced from SiO_2/C predecessor.

ence. A sodium sulfate solution (0.2 M) was used as the electrolyte, and a 300 W Xe lamp ($\lambda = 320$–780 nm) was introduced as the light source. The working electrode was prepared by FTO glass pieces, which was cleaned by sonication in cleanout fluid, acetone and ethanol in sequence. The photocatalyst was dispersed in ethanol under sonication to form a suspension. A photocatalyst film was fabricated by spreading the suspension onto the conductive surface of the FTO glass.

3. Result and discussion

3.1. Crystal phase of SiC

Crystal phase of SiC samples with different carbothermic reduction temperature and time was investigated by XRD, as shown in Fig. 1. When the brown aerogel precursor was calcined at 1673 K, no matter how long the reaction time (5, 8, or 10 h) takes, no SiC crystal phase was formed. The obtained sample only showed a strong diffraction at $2\theta = 21°$, assigning to tridymite phase SiO_2 (JCPDS No. 42-1401). This is also confirmed by the fact that the samples can be completely dissolved as we dispersed samples in 10 wt% NaOH solution. Increasing temperature to 1723 K, SiC started to be formed with three obvious peaks at $2\theta = 35.6°$, $60.0°$ and $71.8°$ in XRD pattern, corresponding to the crystal faces (111), (220), and (311) of cubic structure β-SiC (JCPDS No. 65-0360), respectively. The shoulder peak located at $2\theta = 33°$ (marked with *) may results from the stacking faults in β-SiC [36]. Prolonging the reaction time at this heating temperature can improve the crystallinity of β-SiC with stronger XRD peak intensity. Further increasing temperature to 1773 K, no additional diffraction peaks was observed besides that of β-SiC crystal phase, and the crystallinity of β-SiC was also improved. However, the peak intensity of SiC crystal phase was almost independent of calcination time at 1773 K. Therefore, the β-SiC crystal phase started to form at 1723 K.

3.2. Morphology structure of SiC samples

The SiC samples after the removal of unreacted SiO_2 with 10 wt% NaOH solution treatment were measured by SEM and TEM to investigate its morphology and microstructure, as shown in Fig. 2. The imparity morphologies of hollow microsphere of SiC were observed dependently on the calcined temperature and time. When the precursor was calcined at 1723 K for 8 h, the as-prepared SiC sample displayed the morphology of hollow microspheres with an opened mouth (Fig. 2b). The size of SiC hollow microspheres was about 10 μm. If the calcination time was shortened to 5 h, the as-prepared SiC hollow microspheres were seriously incomplete (Fig. 2a), probably because the shells of the hollow microsphere were rather thin and cannot yet completely form. With increasing calcination time to 10 h, the shells of the hollow microsphere were broken into the hollow half-sphere (Fig. 2c). When the calcination temperature was increased to 1773 K, no whole hollow microspheres of SiC was obtained even the calcination time as short as 5 h (Fig. 2d–f). The shells of hollow SiC microspheres were cracked more and more seriously with increasing reaction time at 1773 K. After calcination at 1773 K for 10 h, the shells were fractured totally into small fragments (Fig. 2f).

Fig. 2g shows that the surface of hollow microspheres for SiC (1723 K, 8 h) samples was rough and the shell was consisted of the aggregation of SiC nanoparticles. The HRTEM images of as-prepared SiC hollow spheres are shown in Fig. 2h. The estimated interplanar space corresponded to be a d-spacing of 0.252 nm. This was consistent with the lattice spacing of the (111) plane in the XRD pattern of β-SiC. Energy dispersive spectroscopy (EDS) measurement (Fig. 2i) implies the presence of Si, C and O with a Si/C molar ratio of 1.16. An excess stoichiometric ratio of Si/C maybe arises from the residual SiO_2.

3.3. Formation processes of SiC hollow spheres

The formation processes of SiC hollow spheres from the sol-gel method and the following carbothermic reduction were observed step by step with SEM and XRD, as shown in Fig. 3. The prepared SiO_2 aerogel prepared from the hydrolysis of TEOS in the presence of P123 and glucose had a perfect spherical shape in SEM images (Fig. 3a). Only one broad diffraction peak was found in the XRD pattern for the aerogel samples (Fig. 3f, line a). The peak centered at $2\theta = 19.8°$ can be attributed to amorphous SiO_2, which was exactly in agreement with the reported results by Pinotti et al. [37] and Rangelova et al. [38], but abundant glucose was silent in XRD pattern. After carbonization of P123 and glucose in aerogel by heating at 823 K for 5 h under N_2 atmosphere, the SiO_2 samples maintained their spherical structure (Fig. 3b). However, the XRD pattern revealed a new broad peak in the range $2\theta = 23$–27° (Fig. 3f, line b). This broad peak was often observed as the (002) diffraction from carbonaceous materials with poor crystallinity [39]. Due to a substantial excess of glucose in the precursor, the diffraction peak of amorphous SiO_2 may be covered up by the strong peak of carbon. With further increasing the heating temperature to 1723 K under flowing Ar atmosphere for the carbothermic reduction of SiO_2, the microspherical structure of samples was still maintained, but some cracks appeared on the sphere surface (Fig. 3c). The XRD pattern (Fig. 3f, line c) showed that the cubic structure of β-SiC started to form as indexed by the three peaks marked with circles. Other small diffraction peaks labelled by triangle and square were attributed to redundant carbon and unreacted quartz SiO_2 (JCPDS No. 47-1144), respectively. It's worth mentioning that the unreacted SiO_2 in this sample differed from neither the amorphous SiO_2 in aerogel nor the crystal SiO_2 (JCPDS No. 42-1401) calcined at 1673 K due to the crystal phase transfer at high temperature. After carbothermic reduction step, the samples were thermally treated under flow-
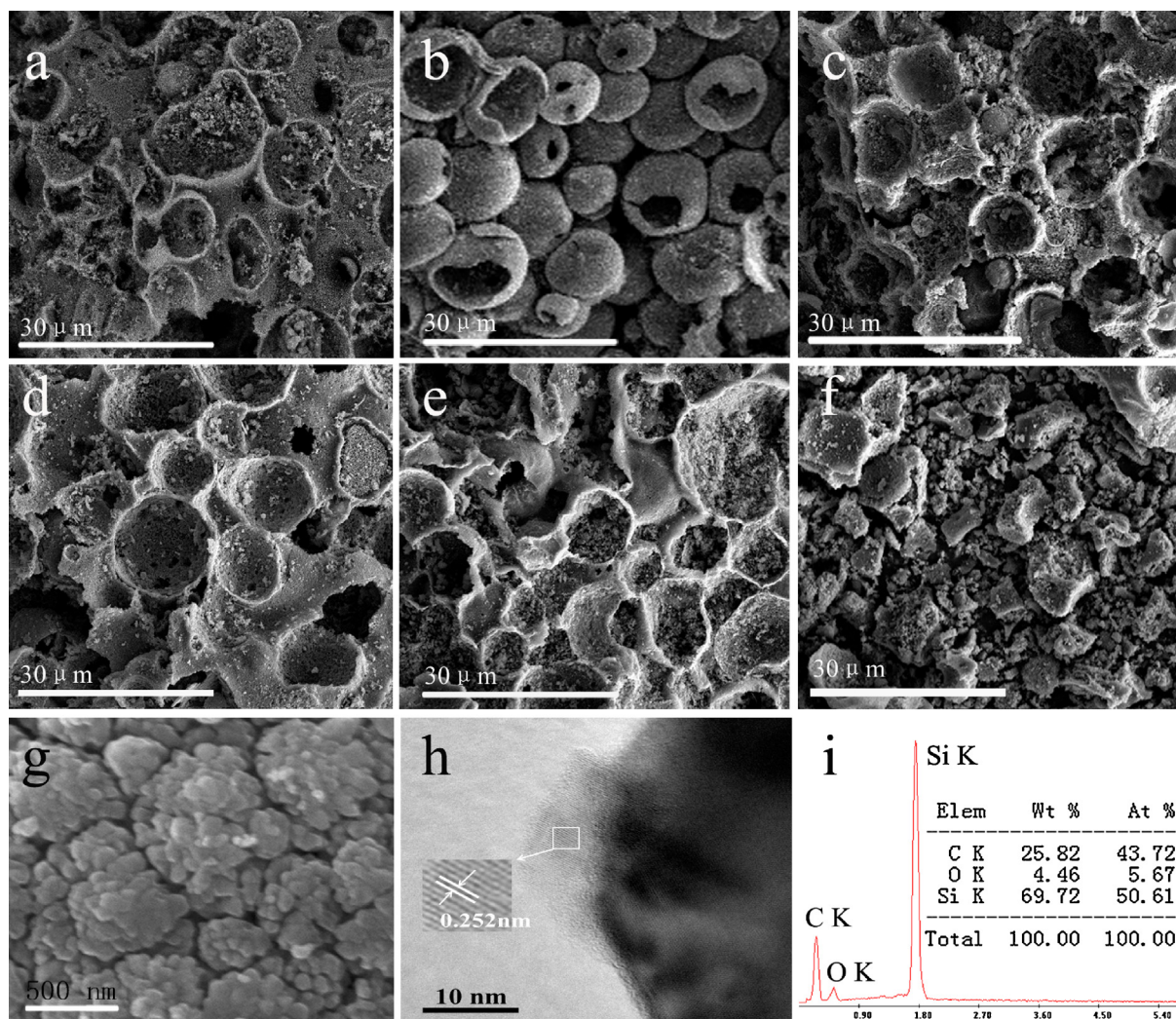
Fig. 2. SEM images of the as-prepared SiC samples obtained in different conditions (a) 1723 K, 5 h; (b, g) 1723 K, 8 h; (c) 1723 K, 10 h; (d) 1773 K, 5 h; (e) 1773 K, 8 h; (f) 1773 K, 10 h. (h) HRTEM image and (i) EDS result of as-prepared SiC 1723 K, 8 h.

ing oxygen at 873 K for 5 h to remove the unreacted carbon. The generated CO_2 gas releasing from confined location in the microsphere broke out the sphere shell and thus led to forming an opened mouth on the shell, as shown in Fig. 3d. Accordingly, the diffraction peak of redundant carbon disappeared in the XRD pattern (Fig. 3f, line d), but the unreacted crystal SiO_2 still remained. Finally, the resulting samples were treated with NaOH solution to remove the unreacted SiO_2. The integrated SiC hollow spheres were observed in SEM image (Fig. 3e). The XRD pattern showed only the sharp diffraction peaks of β-SiC without any other disturbance peaks of impurity (Fig. 3f, line e).

Basing on the above SEM and XRD observations, the growth model of SiC hollow spheres involving five steps was illuminated in Fig. 4. The P123 and glucose were firstly wrapped together to form microsphere as a template [23], and the SiO_2 particles from the TEOS hydrolysis were self-assembled onto the template spherical surface (step 1). And then the P123 and glucose microspheres were

carbonized into carbon spheres with calcination at 823 K under N_2 atmosphere (step 2). Further thermally treating at 1723 K, an interfacial reaction between outer SiO_2 particle and carbon sphere core produced SiC sphere shell (step 3). Following by O_2 calcination at 873 K, the unreacted carbon core was burned out and resulted in an open mouth on the shell of SiC sphere (step 4). Finally, after the outer unreacted SiO_2 was removed with NaOH solution (step 5), the SiC hollow spheres with an open mouth were achieved.

3.4. TG-DSC analysis

To confirm the thermal transformation steps of SiC, thermogravimetric analysis (TGA) of the SiO_2/glucose aerogel were carried out under Ar atmosphere, as shown in Fig. 5 and Table 1. The aerogel samples underwent three weight loss steps when heated from 400 to 1820 K. The first weight loss of 9.3% occurred at temperature below 473 K, corresponding to the evaporation of adsorbed

Table 1
TG analytical data of SiO_2/glucose aerosol predecessor.

Temp. range/K	Experimental TG mass loss/%	Attribution	Calculated mass loss/%	DSC Exo/endo peaks/K
400–473	9.3	Desorption of surface moisture	–	Intensive endo/450
473–823	5.2	Carbonization of P123	5.3	Weak endo/775
823–1723	39.9	Carbonization of glucose	39.1	Intensive exo/1720

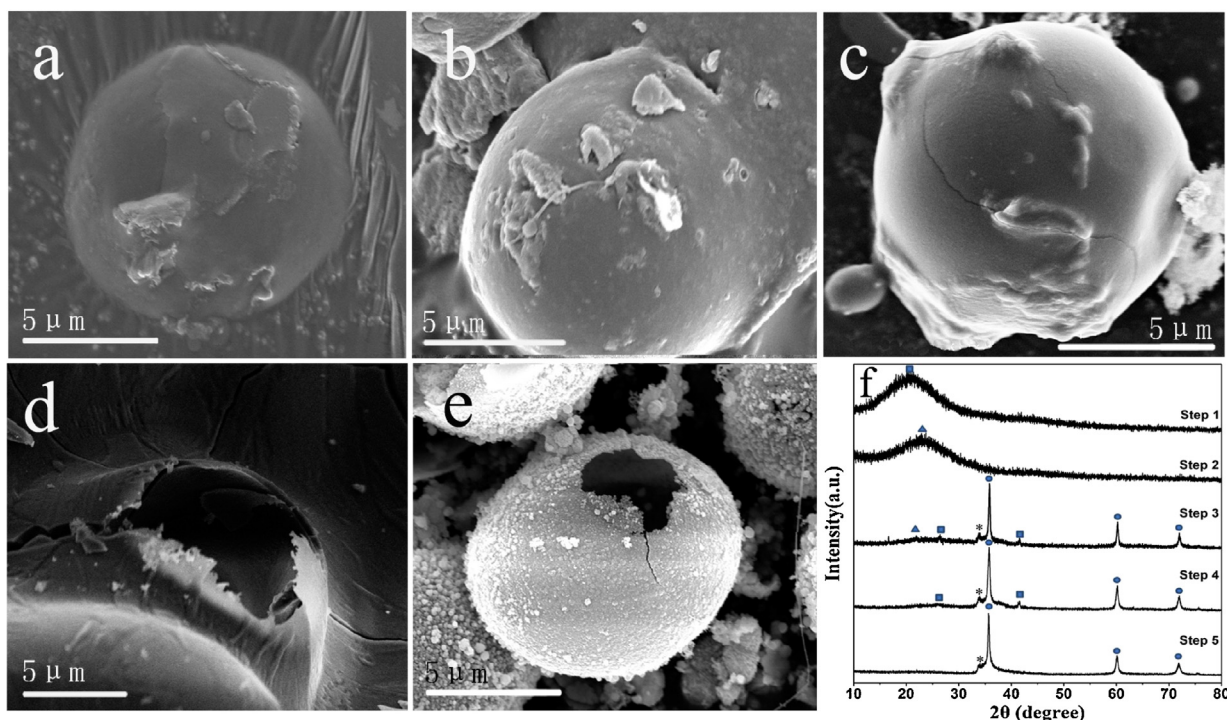**Fig. 3.** SEM images of each process of SiC hollow sphere preparation (a) SiO_2/glocose aerogel; (b) sample after Preliminary carbonization at 823 K for 5 h in nitrogen atmosphere; (c) sample after carbothermic reduction at 1723 K for 8 h in argon atmosphere; (d) sample after calcined at 873 K for 5 h in oxygen atmosphere; (e) as-prepared SiC; and (f) XRD patterns of each process.

ethanol and water from the samples [40]. This produced a sharp endothermic peak at around 450 K of DSC curve. At 473–823 K, a minor mass loss of 5.2% can be seen due to the dehydration decomposition of P123 into carbon with a weak endothermic peak at 775 K at DSC curve [41]. While in the region of 823–1723 K, a major mass loss of 39.9% was observed, which can be attributed to dehydrating of glucose into carbon [42]. When the temperature was higher than 1723 K, no obvious mass loss occurs at TG curve, but an

intensive exothermic peak at exactly 1720 K in DSC curve appeared. This temperature was in accordance with the critical point of SiC crystal formation as indicated by the above XRD investigation. Vix-Guterl et al. also reported that the SiO_2/C material converted into SiC happened at 1700 K heating in an argon flow [43]. Therefore, the exothermic peak at about 1720 K was account for the SiC formation from the reaction between SiO_2 and C.
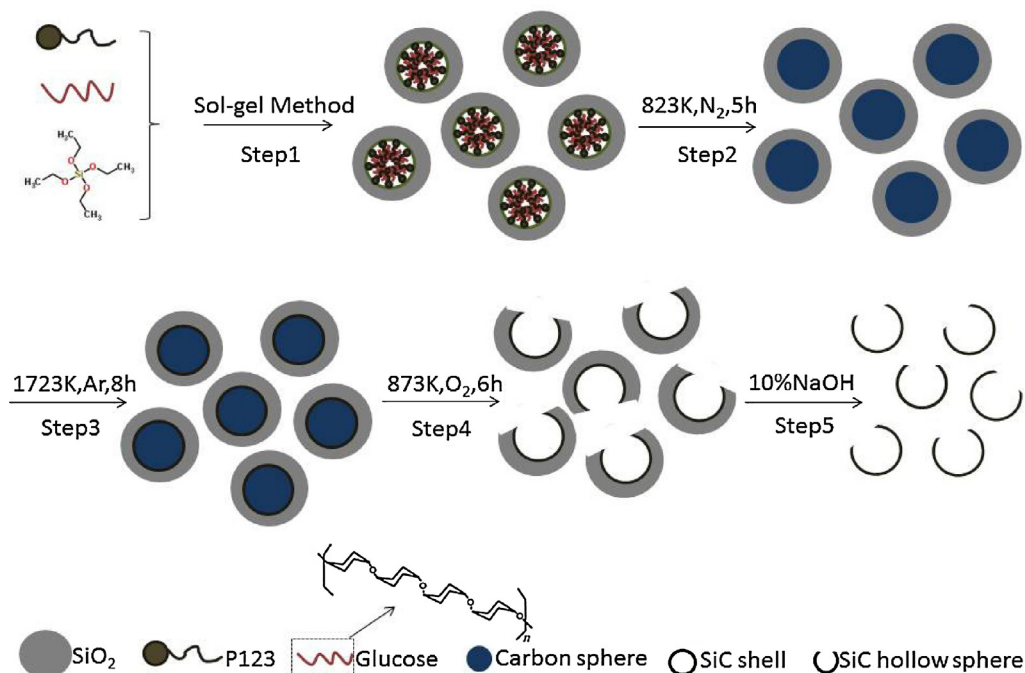

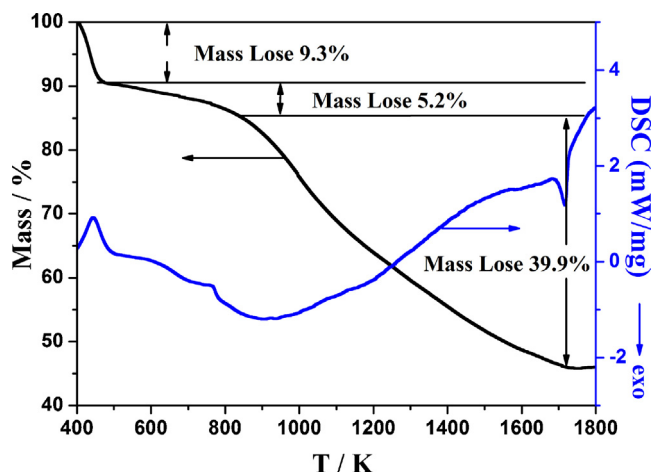**Fig. 4.** Formation processes of SiC hollow sphere.

Fig. 5. TG curves of SiO₂/glucose aerosol predecessor.

The accurate quantitative weight loss (in Table 1) of carbonization processes of both P123 and glucose are calculated according to the weight of raw materials in precursor. The detailed calculation process is illustrated in supplementary information (SI). The calculated weight loss from dehydration decomposition of P123 into carbon was quite consistent with that one from TGA curve in the range of 473–823 K, while the calculated weight loss from dehydration of glucose agreed well with one from 823 to 1723 K. This verifies the above speculated processes of SiC formation at each heating step.

3.5. Optical properties of SiC

The UV–vis diffuse reflectance spectra (Fig. 6a) revealed that the prepared SiC samples can absorb visible light, which was consistent with the typical absorption feature reported for SiC materials [7]. The absorption band edge of SiC samples can be determined by the intercept of spectrum tangent with horizontal axis (F(R) = 0). Both the absorption band edge and band gap of samples are summarized in Table 2. As for the optimal hollow microsphere SiC (1723 K, 8 h), its absorption band edge is 534 nm, corresponding to a band gap of 2.3 eV calculated according to formula (1) [44,45].

Optical energy band gap (eV) = 1240/Optical absorption band edge (nm) (1)

Compared to SiC (1723 K, 8 h), the other SiC samples displayed a blue shift of absorption edges in some degree and thus had a larger band gap. The slight change in the absorption band edge maybe arose from the alteration of morphology or crystal structure of SiC with calcination temperature and time [46,47]. For this purpose, we magnified the main diffraction peak at 35.6° of SiC samples and found a tiny displacement (Fig. 6b). This indicates a structure distortion of inter-planar spacing of SiC by high temperature calcination. Interestingly, the order of absorption band edge is found to be gone adversely with that of diffraction peak for SiC samples. SiC (1723 K, 8 h) had a largest absorption band edge of 534 nm with a smallest diffraction peak at 35.65°. Therefore, the blue shift of absorption band edge was attributed to the little change in crystal structure of SiC with calcination temperature and time.

3.6. Photocatalytic CO₂ reduction on SiC

The conduction band potential of SiC semiconductor was about −1.40 V, far more negative than the reduction potential of CO_2/CH_4 (−0.24 V vs. NHE, pH = 7.0) [48]. It was energetically favorable for electrons from the conduction band of SiC to trigger the reduction of CO_2. Thus, the photoreduction of CO_2 as a model reaction was used to evaluate the photocatalytic performance of the prepared SiC samples.

Fig. 7a shows the average yields of CH_4 over the SiC samples for the CO_2 photoreduction in the presence of H_2O vapor under simulated solar light irradiation for 4 h. CH_4 was detected as a simplex product in SiC reaction system, which was in line with the previous reported work for the CO_2 photoreduction with water vapor [49]. Each of the prepared SiC samples can photocatalytically reduce CO_2 into CH_4, and their activity for CH_4 evolution was markedly better than standard photocatalyst P25 TiO_2. This is due to the unique electronic structure of SiC materials with a very negative conduction band potential of −1.40 V to energetically facilitate the photoexcited electron reduction of CO_2. However, the photocatalytic activity of SiC samples was varied with its calcination temperature and time. As a whole, the SiC samples obtained at 1723 K displayed a better activity than samples at 1773 K do for CH_4 evolution. For samples obtained at 1723 K, the SiC (1723 K, 8 h) sample had a highest photoactivity of CH_4 evolution (28.1 μmol/g). To confirm the photocatalytic process in the CO_2 conversion over SiC, a set of control experiments were performed in absence of either photocatalyst, or light, or H_2O vapor, or CO_2 for photocatalytic reaction under the same experimental conditions (Fig. S1, SI), respectively. No appreciable products were detected in the
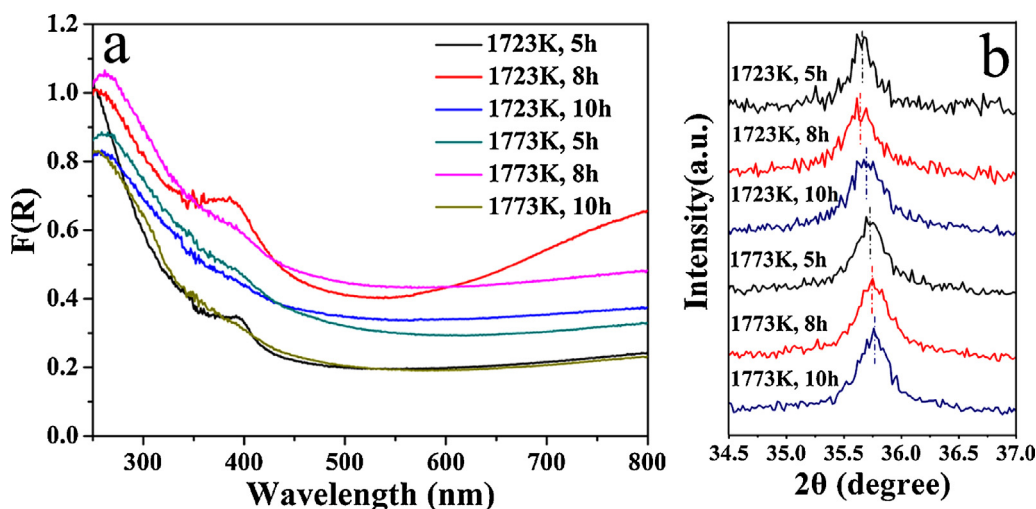

Fig. 6. (a) UV-vis DRS pattern of SiC, (b) Magnified XRD patterns of SiC.

Table 2
The optical absorption band edge and energy band gap of SiC samples.

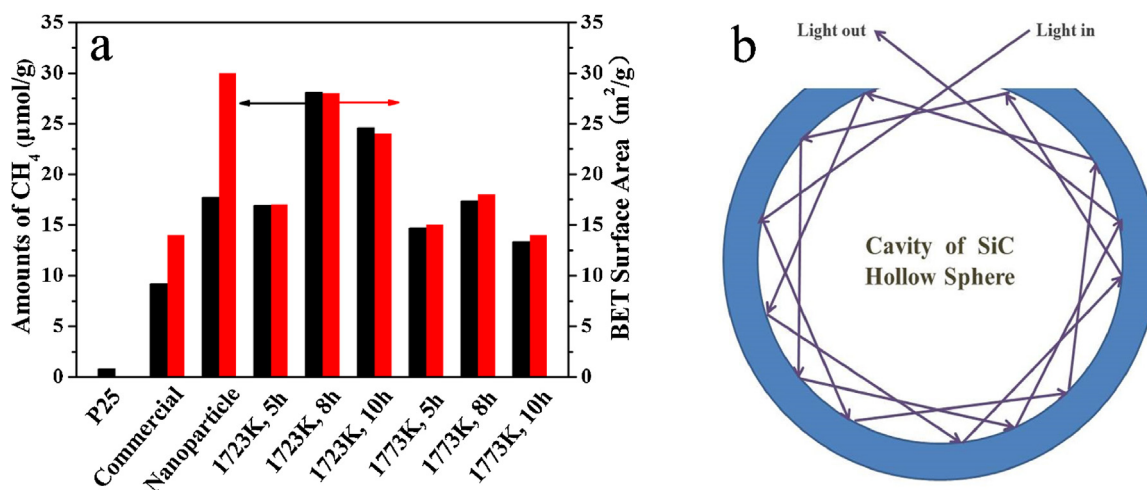| Sample	Optical absorption band edge/nm	Optical energy band gap/eV	Main peak of XRD/degree
1723 K, 5 h	484	2.6	35.67
1723 K, 8 h	534	2.3	35.65
1723 K, 10 h	482	2.6	35.71
1773 K, 5 h	467	2.7	35.73
1773 K, 8 h	464	2.7	35.75
1773 K, 10 h	424	2.9	35.76

Fig. 7. (a) Relationship between BET surface area and CH_4 evolution rate of SiC samples under simulated solar light irradiation for 4 h; (b) Schematic diagram of light reflex inside SiC hollow sphere.
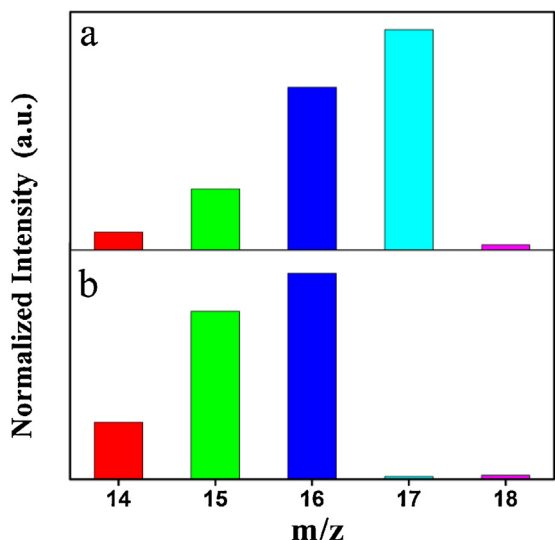

Fig. 8. Mass spectra of the reaction product from (a) $^{13}CO_2$ and H_2O; (b) $^{12}CO_2$ and H_2O over SiC hollow spheres.

absence of either photocatalyst or light irradiation. There was a small amount of product when the reaction was carried out in an anhydrous CO_2 atmosphere. Furthermore, it can be clearly found an inactivation in the reaction without CO_2. All of these findings illustrated that the CO_2 conversion over SiC samples was photocatalytic processes. Isotopic experiments using $^{13}CO_2$ (Fig. 8) clearly show that $^{13}CH_4$ was the main product of the reaction, as revealed by the peak at $m/z = 17$ (further fragmentation results in peaks at $m/z - 1$, $m/z - 2$ and so on). This further confirms the produced CH_4 resulting from CO_2 reduction.

The higher activity of the prepared SiC was related to the higher BET surface area of hollow spherical structure, as compared with commercial SiC. The activity of the different SiC hollow sphere samples was proportional to their BET surface area (Fig. 7a). The higher surface area of SiC samples could facilitate CO_2 adsorption and mass transfer process, and thus improve photocatalytic CO_2 reduction. On the other hand, the hollow sphere structure can also account for the good photocatalytic performance of SiC for CO_2 reduction. The hollow sphere structure allowed multi-reflections of illumination light within its interior cavities, resulting in more efficient use of the light source and enhanced photocatalytic activity[50]. To confirm the light multi-reflection effect of hollow spherical structure, we prepared the nanoparticle SiC samples with similar BET surface area and used them for photocatalytic CO_2 reduction. It clearly showed that hollow sphere SiC (1723 K, 8 h) samples had a much better activity than SiC nanoparticle does (Fig. 7a). This evidences the light multi-reflection in hollow sphere structure of SiC also enhance photocatalytic CO_2 conversion (Fig. 7b).

In order to further improve efficiency of CH_4 evolution, various contents of Pt cocatalyst were introduced to the surface of SiC. The X-ray diffraction peak of Pt was found in the patterns of Pt/SiC samples (Fig. S2, SI). The TEM images of 2 wt% Pt/SiC confirmed that the Pt nanoparticles distributed uniformly on the surface of SiC with a size of 2–4 nm (Fig. S3, SI). In addition, X-ray photoelectron spectroscopy images (Fig. S4, SI) can also confirm the existence of metal Pt. Fig. 9a recorded the various amount of Pt cocatalyst loading on SiC (1723 K, 8 h) for CO_2 photoreduction in the presence of H_2O vapor under simulated solar light irradiation for 4 h. Either 1 wt% or 2 wt% or 3 wt% Pt loading can indeed further enhance CH_4 evolution on SiC. However, the 2 wt% Pt/SiC sample showed the highest activity of CH_4 evolution of 67.2 μmol/g (corresponding to 16.8 μmol/g/h or 376.4 μl/g/h), which is over 2 times higher than that of the bare SiC (28.1 μmol/g). This activity of Pt/SiC for CH_4 evolution is higher than that of many reported metal oxides under
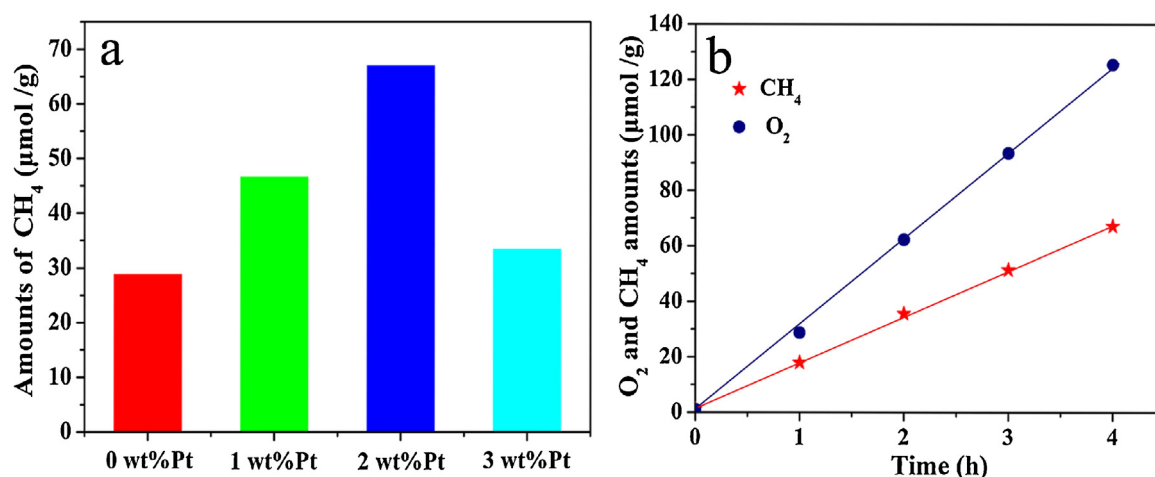
Fig. 9. (a) CH_4 evolution rate of the bare SiC and Pt/SiC samples under simulated solar light irradiation for 4 h; (b) CH_4 and O_2 evolution rate of 2wt%Pt/SiC under simulated solar light.
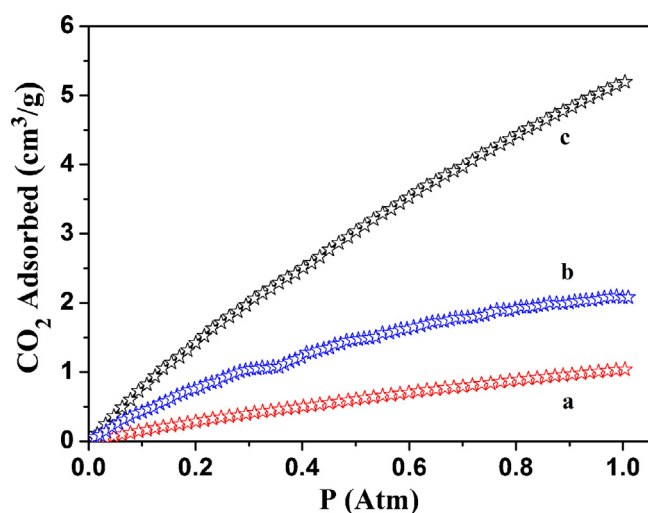

Fig. 10. CO_2 adsorption isotherms of (a) commercial SiC, (b) SiC hollow sphere, and (c) 2 wt% Pt/SiC hollow sphere.
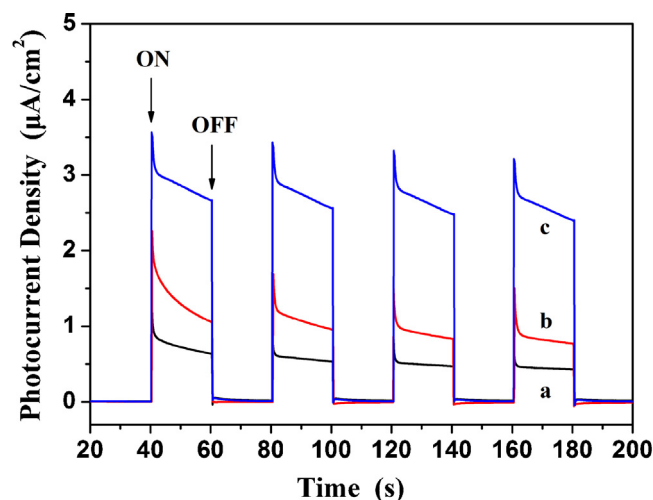
Fig. 11. Photocurrent of (a) commercial SiC, (b) SiC hollow sphere, and (c) 2 wt% Pt/SiC hollow sphere.

similar experimental conditions, such as Pt/TiO_2 [51], CdS/WO_3 [52], Zn_2GeO_4 [53], CeO_2 [54] and g-C_3N_4/$NaNbO_3$ [55]. Moreover, the CH_4 product evolution over 2 wt% Pt/SiC sample exhibited linear growth (Fig. 9b), indicating a stable reactivity of CO_2 reduction. It is believed that CO_2 could react with H_2O through two respective half reactions with photogenerated electrons and hole to simultaneously produce CH_4 and O_2 in an ideal process [56]. A continuous O_2 release process from water oxidation should contribute to the above phenomenon.

To investigate the contributions of BET surface area or hollow spherical structure or Pt cocatalysts to the CO_2 conversion over SiC samples, CO_2 adsorption and photocurrent and photoluminescence spectra were employed to characterize different SiC samples. Fig. 10 showed the CO_2 adsorption isotherms of 2 wt% Pt/SiC hollow sphere, bare SiC hollow sphere and commercial SiC samples. The bare SiC hollow sphere displayed a better ability of capturing CO_2 than commercial SiC, because of its higher BET surface area. Pt loading markedly enhanced the adsorption capability for CO_2, implying that the Pt particles on SiC could induce a certain extent of the CO_2 adsorption. The enhanced CO_2 adsorption capacity is due to the dissociative adsorption of CO_2 on Pt cocatalyst, which is consistent with many reported studies in CO_2 absorption on Pt-based samples [57,58]. An increase of adsorption capability for CO_2 over

SiC hollow sphere can therefore facilitate the mass transfer process and play an important role in the higher CO_2 photoreduction activity.

Photocurrent response was measured under Xe lamp irradiation, as shown in Fig. 11. The hollow spherical SiC showed higher cathodic photocurrent than bulk SiC sample. This indicates that the more excited state electrons over hollow spherical SiC can be generated and separated quickly. This can be well explained by the hollow sphere structure allowed multi-reflections of illumination light within its interior cavities resulting in more efficient use of the light source, and thus enhancement of the concentration of excited state electrons on SiC hollow sphere. As expected, the deposition of Pt considerably increased the photocurrent response of SiC hollow sphere. This is because of the formation of Schottky barriers at the Pt/SiC interface to improve the transfer of photogenerated electrons from SiC to the surface Pt particles [59]. The photoluminescence spectra (Fig. S5, SI) in well agreement with photocurrent results further confirmed the hollow spherical structure and Pt deposition can efficiently generate and separate photogenerated charge carriers on SiC samples. Therefore, both high BET surface area and hollow spherical structure are contributed to a high activity for CO_2 photocatalytic conversion. Moreover, Pt cocatalysts not only facilitated the separation of photogenerated electrons on SiC, but also
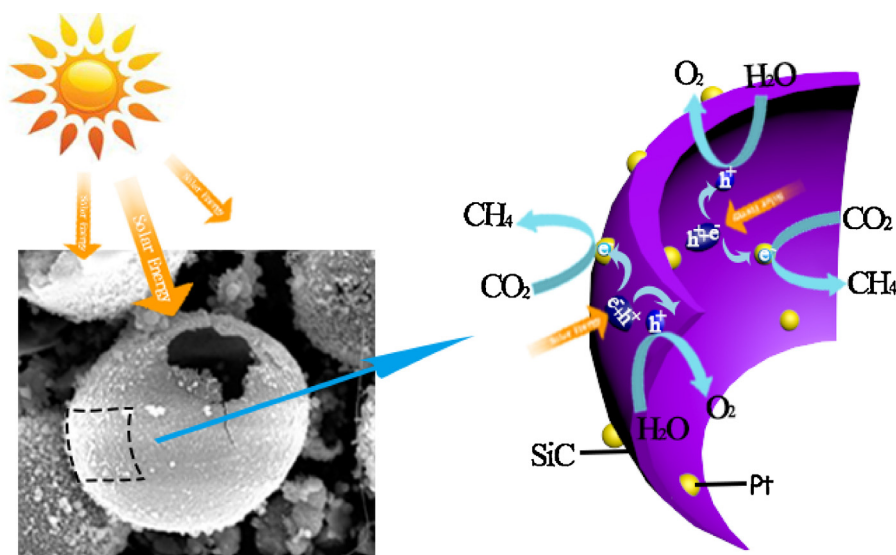
Fig. 12. Schematic illustration of the charge transfer in Pt/SiC hollow spheres for CO_2 reduction with H_2O to CH_4 under simulated solar light illumination.

increased CO_2 adsorption capability, both of which led to a high efficiency for CO_2 conversion over Pt/SiC.

On the basis of the above results, a mechanism of photocatalytic reduction of CO_2 over the Pt/SiC hollow sphere sample was delineated in Fig. 12. Upon irradiation, the photoexcitation of electrons took place from the valence band to the conduction band of SiC on both inner and outer surface, leaving holes in the valence band. With the modification of Pt nanoparticles, the effective interface was formed between Pt and SiC. The photogenerated electrons from SiC were then migrated to the Pt owing to the lower Fermi level of Pt. Seeing that CO_2 molecules can be easily adsorbed on the surface of Pt, the reaction between activated CO_2 and electrons occurs over Pt nanoparticles to form superoxide ($\bullet CO_2{}^-$) radicals. It is widely known that the reduction of CO_2 involves an 8-electron process to form CH_4. The enriched electron density on the Pt favored the photoreduction of CO_2 to CH_4 through a series of radical reactions. Meanwhile, the photo induced holes on SiC reacted with H_2O molecules to produce O_2. As a result, the high photocatalytic performance of Pt/SiC was achieved on account of the intimate interfacial contact formation between Pt and SiC hollow spheres. The synergistic effect between Pt and SiC not only significantly enhanced the electrical conduction efficiency, but also promoted the separation of electron-hole pairs, thereby leading to an improved photocatalytic activity.

4. Conclusions

We developed a simple P123 and glucose assisted sol-gel methods to successfully prepare SiC hollow microsphere with an opened mouth. The perfect hollow sphere structure SiC with BET surface area of $28 m^2/g$ can be achieved by carbothermal reduction of aerogel at 1723 K for 8 h under flowing Ar. The P123 and glucose wrapped together to form microsphere as a template for the reaction with the self-assembled SiO_2 particle on surface can contribute to the hollow sphere structure of SiC. The unique electronic structure, hollow microsphere and high BET surface area together led to a marked enhancement of photocatalytic activity for the prepared SiC toward CO_2 reduction with H_2O vapor into CH_4. Moreover, the photocatalytic activity for the prepared SiC can be further improved by loading Pt cocatalyst. The optimal 2.0 wt% Pt loading produced a stable CH_4 evolution rate as high as 67.2 μmol/g under simulated solar light irradiation for 4 h. These findings provide a new method in the preparation of thermally and chemically stable non-metallic carbide with unique hollow spherical structure, but also highlight the photocatalytic application of the carbide materials for CO_2 reduction into hydrocarbons.

Appendix A. Supplementary data

Supplementary data associated with this article can be found, in the online version, at http://dx.doi.org/10.1016/j.apcatb.2017.01.028.

References

[1] R. Kuriki, K. Sekizawa, O. Ishitani, K. Maeda, Angew. Chem. Int. Ed. Engl. 54 (2015) 2406–2409.
[2] Y. Fu, D. Sun, Y. Chen, R. Huang, Z. Ding, X. Fu, Z. Li, Angew. Chem. Int. Ed. Engl. 51 (2012) 3364–3367.
[3] I. Hod, M.D. Sampson, P. Deria, C.P. Kubiak, O.K. Farha, J.T. Hupp, ACS Catal. 5 (2015) 6302–6309.
[4] H. Fei, M.D. Sampson, Y. Lee, C.P. Kubiak, S.M. Cohen, Inorg. Chem. 54 (2015) 6821–6828.
[5] T. Arai, S. Sato, T. Morikawa, Energy Environ. Sci. 8 (2015) 1998–2002.
[6] W. Lu, D. Wang, L. Guo, Y. Jia, M. Ye, J. Huang, Z. Li, Y. Peng, W. Yuan, X. Chen, Adv. Mater. 27 (2015) 7986–7991.
[7] Y. Peng, Z. Guo, J. Yang, D. Wang, W. Yuan, J. Mater. Chem. A 2 (2014) 6296.
[8] L. Chen, Y. Wang, J. Rao, Y. Zhou, Int. J. Appl. Ceram. Technol. 12 (2015) 184–191.
[9] S. Safi, A. Kazemzadeh, Ceram. Intern 39 (2013) 81–86.
[10] Y. Nariki, Y. Inoue, K. Tanaka, J. Mater. Sci. 25 (1990) 3101–3104.
[11] M. Wang, J. Chen, X. Liao, Z. Liu, J. Zhang, L. Gao, Y. Li, Int. J. Hydrogen Energy 39 (2014) 14581–14587.
[12] M.A. Gondal, M.A. Ali, X.F. Chang, K. Shen, Q.Y. Xu, Z.H. Yamani, J. Environ. Sci. Health Part A Tox. Hazard. Subst. Environ. Eng. 47 (2012) 1571–1576.
[13] L. Li, J. Niu, Y. Yang, Z. Xia, Comput. Mater. Sci. 83 (2014) 255–260.
[14] S. Sharma, J. Prakash, K. Sudarshan, D. Sen, S. Mazumder, P. Pujari, Macromolecules 48 (2015) 5706–5713.
[15] M. Taghavi, E. Ghasemi, A. Monshic, J. Ceram. Process. Res. 15 (2014) 242–245.
[16] G. Xu, K. Wang, Z. Zhong, C.-s. Chen, P.A. Webley, H. Wang, J. Mater. Chem. A 2 (2014) 5841–5846.

[17] Y. Zhang, X. Han, K. Zheng, Z. Zhang, X. Zhang, J. Fu, Y. Ji, Y. Hao, X. Guo, Z.L. Wang, Adv. Funct. Mater. 17 (2007) 3435–3440.
[18] S. Li, Y. Zhang, J. Han, Y. Zhou, Ceram. Int. 39 (2013) 449–455.
[19] J. Lin, X. Zhang, W. Han, H. Jin, Mater. Sci. Eng.: A 551 (2012) 187–191.
[20] M.K. Mani, G. Viola, M.J. Reece, J.P. Hall, S.L. Evans, Mater. Sci. Eng.: A 592 (2014) 19–27.
[21] M. Yazdanfar, I.G. Ivanov, H. Pedersen, O. Kordina, E. Janzén, J. Appl. Phys. 113 (2013) 223502.
[22] H. Wang, J.-S. Yu, X.-D. Li, D.-P. Kim, Chem. Commun. (2004) 2352–2353.
[23] K. Wang, H. Wang, Y.B. Cheng, Chem. Commun. 46 (2010) 303–305.
[24] Y. Zhang, E.-W. Shi, Z.-Z. Chen, X.-B. Li, B. Xiao, J. Mater. Chem. 16 (2006) 4141–4145.
[25] G. Shen, D. Chen, K. Tang, Y. Qian, S. Zhang, Chem. Phys. Lett. 375 (2003) 177–184.
[26] X. Zhou, Y. Liu, X. Li, Q. Gao, X. Liu, Y. Fang, Chem. Commun. 50 (2014) 1070–1073.
[27] B. Moshtaghioun, R. Poyato, F. Cumbrera, S. de Bernardi-Martin, A. Monshi, M. Abbasi, F. Karimzadeh, A. Dominguez-Rodriguez, J. Eur. Ceram. Soc. 32 (2012) 1787–1794.
[28] B. Moshtaghioun, A. Monshi, M. Abbasi, F. Karimzadeh, Int. J. Refract. Met. Hard Mater. 29 (2011) 645–650.
[29] S. El-Sheikh, Z. Zaki, Y. Ahmed, J. Alloys Compd. 613 (2014) 379–386.
[30] M. Yazdanfar, H. Pedersen, P. Sukkaew, I.G. Ivanov, Ö. Danielsson, O. Kordina, E. Janzén, J. Cryst. Growth 390 (2014) 24–29.
[31] S. Zhang, Q. Xu, R. Tu, T. Goto, L. Zhang, J. Am. Ceram. Soc. 98 (2015) 236–241.
[32] J. Ding, H. Zhu, G. Li, C. Deng, J. Li, Appl. Surf. Sci. 320 (2014) 620–626.
[33] A. Maity, H. Das, D. Kalita, N. Kayal, T. Goswami, O. Chakrabarti, J. Eur. Ceram. Soc. 34 (2014) 3499–3511.
[34] X. Qi, G. Zhai, J. Liang, S. Ma, X. Liu, B. Xu, CrystEngComm 16 (2014) 9697–9703.
[35] J. Hu, M. Chen, X. Fang, L. Wu, Chem. Soc. Rev. 40 (2011) 5472–5491.
[36] W.S. Seo, K. Koumoto, S. Aria, J. Am. Ceram. Soc. 83 (2000) 2584–2592.
[37] A. Pinotti, M. García, M. Martino, N. Zaritzky, Food Hydrocolloids 21 (2007) 66–72.
[38] N. Rangelova, L. Radev, S. Nenkova, I.M. Miranda Salvado, M.H. Vas Fernandes, M. Herzog, Cent. Eur. J. Chem. 9 (2010) 112–118.
[39] Z. Ma, T. Kyotani, A. Tomita, Chem. Commun. (2000) 2365–2366.
[40] D.-H. Wang, L. Jia, X.-L. Wu, L.-Q. Lu, A.-W. Xu, Nanoscale 4 (2012) 576–584.
[41] S.-Y. Chen, T. Mochizuki, Y. Abe, M. Toba, Y. Yoshimura, P. Somwongsa, S. Lao-ubol, Appl. Catal. B: Environ. 181 (2016) 800–809.
[42] Z.-Z. Jiang, Z.-B. Wang, Y.-Y. Chu, D.-M. Gu, G.-P. Yin, Energy Environ. Sci. 4 (2011) 2558–2566.
[43] C. Vix-Guterl, I. Alix, P. Ehrburger, Acta Mater. 52 (2004) 1639–1651.
[44] X. Chen, L. Liu, Y.Y. Peter, S.S. Mao, Science 331 (2011) 746–750.
[45] M.M. Khan, S.A. Ansari, D. Pradhan, M.O. Ansari, D.H. Han, J. Lee, M.H. Cho, J. Mater. Chem. A 2 (2014) 637–644.
[46] J.-Y. Hao, Y.-Y. Wang, X.-L. Tong, G.-Q. Jin, X.-Y. Guo, Catal. Today 212 (2013) 220–224.
[47] X.-H. Sun, C.-P. Li, W.-K. Wong, N.-B. Wong, C.-S. Lee, S.-T. Lee, B.-K. Teo, J. Am. Chem. Soc. 124 (2002) 14464–14471.
[48] T. Inoue, A. Fujishima, S. Konishi, K. Honda, Nature 277 (1979) 637–638.
[49] S. Zhu, S. Liang, Y. Tong, X. An, J. Long, X. Fu, X. Wang, Phys. Chem. Chem. Phys. 17 (2015) 9761–9770.
[50] J. Qian, P. Liu, Y. Xiao, Y. Jiang, Y. Cao, X. Ai, H. Yang, Adv. Mater. 21 (2009) 3663–3667.
[51] B. Fang, A. Bonakdarpour, K. Reilly, Y. Xing, F. Taghipour, D.P. Wilkinson, ACS Appl. Mater. Interfaces 6 (2014) 15488–15498.
[52] J. Jin, J. Yu, D. Guo, C. Cui, W. Ho, Small 11 (2015) 5262–5271.
[53] Q. Liu, Y. Zhou, J. Kou, X. Chen, Z. Tian, J. Gao, S. Yan, Z. Zou, J. Am. Chem. Soc. 132 (2010) 14385–14387.
[54] P. Li, Y. Zhou, Z. Zhao, Q. Xu, X. Wang, M. Xiao, Z. Zou, J. Am. Chem. Soc. 137 (2015) 9547–9550.
[55] H. Shi, G. Chen, C. Zhang, Z. Zou, ACS Catal. 4 (2014) 3637–3643.
[56] M. Li, P. Li, K. Chang, T. Wang, L. Liu, Q. Kang, S. Ouyang, J. Ye, Chem. Commun. 51 (2015) 7645–7648.
[57] K.-P. Yu, W.-Y. Yu, M.-C. Kuo, Y.-C. Liou, S.-H. Chien, Appl. Catal. B: Environ. 84 (2008) 112–118.
[58] N. Umezawa, H.H. Kristoffersen, L.B. Vilhelmsen, B. Hammer, J. Phys. Chem. C 120 (2016) 9160–9164.
[59] A.O.T. Patrocinio, J. Schneider, M.D. França, L.M. Santos, B.P. Caixeta, A.E.H. Machado, D.W. Bahnemann, RSC Adv. 5 (2015) 70536–70545.